Mode coupling in $\mathcal{PT}$-symmetric photonic crystals with a flat band

Zhenzhen Liu,[1] Qiang Zhang,[1] Feifei Qin,[1] Yuntian Chen,[2] and Jun Jun Xiao[1,*]

[1]*Shenzhen Engineering Laboratory of Aerospace Detection and Imaging, College of Electronic and Information Engineering, Harbin Institute of Technology (Shenzhen), Shenzhen 518055, China*

[2]*School of Optical and Electronic Information and Wuhan National Laboratory of Optoelectronics, Huazhong University of Science and Technology, Wuhan, China*

(Received 28 May 2018; published 23 October 2018)

The exploration of photonic systems embracing the concept of parity-time ($\mathcal{PT}$) symmetry has become highly active in recent years. Studies on this topic potentially have significant technological implications, enabling unidirectional transmission in optical systems with unusual states of light. Here, we investigate the existence of a flat band in a two-dimensional photonic crystal and the consequences in the context of $\mathcal{PT}$ symmetry. The flat band is ascribed to a pair of two dipolar states and a monopolar state, which is verified by the proposed coupled mode equations. This flat band is protected by the interactions of these three states; therefore it has tremendous potential to investigate the localized stationary eigenstates, and gives rise to intriguing modulations under the perturbation of gain and loss. Especially, gain-loss configurations predominantly act on the coupling behavior of originally orthogonal states, including thresholdless $\mathcal{PT}$ transition, absence, and emergence of $\mathcal{PT}$ transition. The gain-loss configurations, together with the flat band, determine the peculiar band structures and the resultant interesting transmission phenomena. By means of coupled mode equations, we disclose the dynamics upon the perturbation of the gain and loss and the wave vector, and show various transmission modulations including unidirectional behavior.

DOI: 10.1103/PhysRevA.98.043844

I. INTRODUCTION

The notion of flat band dispersions is a promising tool, which is aimed at slow light with zero group velocity and a high density of states [1–3]. Furthermore, flat bands are typical characteristics of localized stationary eigenstates that are extremely sensitive to disorder effects. There have been several attempts to construct a flat band with Hermitian potential, such as Lieb [4] and honeycomb [5] lattices. Extended to the non-Hermitian Hamiltonian, many studies offer diverse routes for achieving an entire flat band [6–8]. As a major subset of non-Hermitian systems, parity-time- ($\mathcal{PT}$-) symmetric systems have attracted significant interest in past decades; they are invariant under the combined action of a parity- and time-reversal operation [9–13]. Significantly, the exceptional point (EP) [14–16] acts as the transition between the $\mathcal{PT}$-symmetric and -broken phases, which raises a variety of intriguing applications, including lasing [17,18], unidirectional transmission [19,20], and sensing [21,22]. Up to now, the constructions of the flat band have been widely investigated in a variety of platforms, especially the non-Hermitian systems. To well understand the natural properties of the flat band in the context of $\mathcal{PT}$ symmetry, a simple photonic crystal with a square lattice serves as an excellent platform to investigate the properties of flat bands and their non-Hermitian behavior under the perturbation of gain and loss.

In this paper, we investigate the formation of a flat band residing in the degeneracy of dipolar states in $\mathcal{PT}$-symmetric photonic crystals (PCs) with square lattice. These two degenerate states are orthogonal along every direction of the Brillouin zone (BZ), which accounts for the existence of the flat band. The formation of this flat band can be predicted and verified by our proposed perturbation method, known as coupled mode formalism. Moreover, when the gain and loss are turned on, the coupling behavior of the induced modes is greatly influenced. Based on the forms of the non-Hermiticity, this flat band would significantly affect the $\mathcal{PT}$-symmetric phase transition and transmission dynamics.

The paper is organized as follows: In Sec. II, we formulate the coupled mode equation based on the perturbative method $\mathbf{k}\cdot\mathbf{p}$. Then the proposed equations are applied to design the flat band protected by the interactions of two degenerate dipolar modes and a monopolar state, and the mode coupling behaviors induced by the $\mathcal{PT}$-symmetric potentials are illustrated in Sec. III in detail. In Sec. IV, the associated transmission properties are given. Finally, our conclusions are drawn in Sec. V.

II. FORMULATION OF MULTIPLE COUPLED MODES

To understand the coupling mechanism induced by the perturbation of wave vector and non-Hermiticity, one must calculate the band structure of the PCs [23], whose fields satisfy the following Maxwell equations:

$$\nabla \times \mathbf{E}(\mathbf{r}) = -j\omega\mu_0\mu\mathbf{H}(\mathbf{r}), \tag{1}$$

$$\nabla \times \mathbf{H}(\mathbf{r}) = j\omega\epsilon_0\varepsilon(\mathbf{r})\mathbf{E}(\mathbf{r}), \tag{2}$$

*eiexiao@hit.edu.cn

where $\varepsilon(\mathbf{r})$ is the relative permittivity function of the PCs, and j the imaginary unit. Due to the lattice vector $\{\mathbf{a}\}$, $\varepsilon(\mathbf{r}) = \varepsilon(\mathbf{r}+\mathbf{a})$, then the Bloch states can be expressed as $E_{n\boldsymbol{k}}(\mathbf{r}) = u_n(\mathbf{r})\exp(-j\mathbf{k}\cdot\mathbf{r})$, where n denotes the band index [24,25]. The periodic function $u_n(\mathbf{r})$ and the corresponding eigenfrequency $\omega_n(\mathbf{k})$ can be obtained from Eqs. (1) and (2). If we turn on the gain and loss, $\varepsilon(\mathbf{r})$ is transformed into $\varepsilon_r(\mathbf{r}) + j\varepsilon_i(\mathbf{r})$, where $\varepsilon_r(\mathbf{r})$ and $\varepsilon_i(\mathbf{r})$ correspond to the Hermitian dielectric function and non-Hermiticity potential function, respectively.

We aim at probing the behavior of the band structure either under the perturbation of gain and loss $\varepsilon_i(\mathbf{r})$ or in the vicinity of the particular $\mathbf{k}_0$ points. Based on the typical perturbation method $\mathbf{k}\cdot\mathbf{p}$, the perturbed eigenfunctions in the vicinity of $\mathbf{k}_0$ can be written as the linear combination of the unperturbed eigenstates. Thus, we construct a model Hamiltonian using the Hermitian Bloch states at the fixed value of wave vector $\mathbf{k}_0$ as a basis. To do so, we expand the Bloch wave functions of the $\mathcal{PT}$-symmetric system as

$$\mathbf{E}'_k(\mathbf{r}) = \tilde{\mathbf{e}}(\mathbf{r})\exp(-j\mathbf{k}\cdot\mathbf{r}), \tag{3}$$

$$\mathbf{H}'_k(\mathbf{r}) = \tilde{\mathbf{h}}(\mathbf{r})\exp(-j\mathbf{k}\cdot\mathbf{r}), \tag{4}$$

with $\tilde{e}(\mathbf{r}) = \sum_{n=1}^{\infty}\alpha_n\tilde{e}_n(\mathbf{r})$ and $\tilde{h}(\mathbf{r}) = \sum_{n=1}^{\infty}\alpha_n\tilde{h}_n(\mathbf{r})$ the periodic function in a unit cell wherein $\tilde{\mathbf{e}}_n = \mathbf{E}_{n,\mathbf{k}_0}e^{j\mathbf{k}_0\cdot\mathbf{r}} = (e_{n,x}, e_{n,y}, e_{n,z})$ and $\tilde{\mathbf{h}}_n = \mathbf{H}_{n,\mathbf{k}_0}e^{j\mathbf{k}_0\cdot\mathbf{r}} = (h_{n,x}, h_{n,y}, h_{n,z})$ [25–27]. To get the concrete formalism, further manipulations are taken as follows, and * denotes the complex conjugate operator. Upon substituting these expansions [Eqs. (3) and (4)] into Eqs. (1) and (2), and multiplying through by $\mathbf{H}^*_{m,\mathbf{k}_0}(\mathbf{r})$ on Eq. (1), and $\mathbf{E}^*_{m,\mathbf{k}_0}(\mathbf{r})$ on Eq. (2), we get two isolated equations labeled as f_1, f_2, respectively. Alternatively, upon substituting $\mathbf{H}^*_{m,\mathbf{k}_0}(\mathbf{r})$ and $\mathbf{E}^*_{m,\mathbf{k}_0}(\mathbf{r})$ into Eqs. (1) and (2), and multiplying through by $\mathbf{H}'_{\mathbf{k}}(\mathbf{r})$ on Eq. (1), and $\mathbf{E}'_{\mathbf{k}}(\mathbf{r})$ on Eq. (2), we get the other two isolated equations labeled as f_3, f_4, respectively. We deliberately handle these four equations by $f_3 - f_1 + f_2 - f_4$ and integrating over the unit cell; naturally it yields the following function:

$$\sum_n \alpha_n[b_{mn} + j(\omega+\omega_m)p_{mn} + j\omega q_{mn} + j(\mathbf{k}-\mathbf{k}_0)\cdot\boldsymbol{\kappa}_{mn}] = 0, \tag{5}$$

where ω_m is the frequency of the mth band of the Hermitian system when the wave vector is fixed at $\mathbf{k}_0$. Given that all perturbation is absent, i.e., $\varepsilon_i(\mathbf{r}) = 0$ and $\mathbf{k} = \mathbf{k}_0$, we shall have the following relation: $b_{mn} = -j(\omega_n+\omega_m)p_{mn}$. Substituting this relation into Eq. (5) yields

$$\sum_n \alpha_n[(\omega-\omega_n)p_{mn} + \omega q_{mn} + (\mathbf{k}-\mathbf{k}_0)\cdot\boldsymbol{\kappa}_{mn}] = 0. \tag{6}$$

For simplicity, the subscript $\mathbf{k}_0$ is omitted in the following demonstration. The element q_{mn} of matrix $\mathbf{Q}$ denotes modal coupling due to the presence of gain and loss in the unit cell:

$$q_{mn} = \int dV(j\varepsilon_i(\mathbf{r})\mathbf{E}_m\cdot\mathbf{E}^*_n), \tag{7}$$

The value of q_{mn} can be simply determined by the symmetry of the fields distribution and the gain-loss distribution. Besides the inversion symmetry, the rotational symmetry of gain-loss distribution can also lead to the absence of q_{mn} [28].

While the element $\boldsymbol{\kappa}_{mn}$ of matrix $\mathbf{k}$ describes the coupling strength for the given $\mathbf{k}$ direction, with $\boldsymbol{\kappa}_{mn}$ given as follows,

$$\boldsymbol{\kappa}_{mn} = \int dV(\mathbf{H}^*_n\times\mathbf{E}_m - \mathbf{E}^*_n\times\mathbf{H}_m), \tag{8}$$

and the element p_{mn} of matrix $\mathbf{P}$ meets the normalization conditions,

$$p_{mn} = \int dV[\varepsilon_r(\mathbf{r})\mathbf{E}_m\cdot\mathbf{E}^*_n + \mu(\mathbf{r})\mathbf{H}_m\cdot\mathbf{H}^*_n]. \tag{9}$$

Obviously, matrix $\mathbf{P}$ must be diagonal, and can be normalized to be the identity matrix due to the orthogonal properties of the isolated band states [26,29], i.e., $\int dV[\varepsilon_r(\mathbf{r})\mathbf{E}_m\cdot\mathbf{E}^*_n + \mu(\mathbf{r})\mathbf{H}_m\cdot\mathbf{H}^*_n] = \delta_{mn}$.

Up to now, we have constructed the coupled mode equation, Eq. (6), which offers us a simple scheme to investigate the band structures of the $\mathcal{PT}$-symmetric PCs as a function of non-Hermiticity and the offset of the wave vector. It is helpful for us to understand the roles played by various non-Hermitian potentials in determining the phase. The existence of a nonzero q_{mn} or $\boldsymbol{\kappa}_{mn}$ illustrates an attractive interaction between two bands, which results in the presence of an EP.

The perturbation of the gain and loss plays a significant role in the coupling effects among the adjacent bands of the original Hermitian systems originating from the nonzero coupling strength between the concerned states defined by Eq. (7). Generally speaking, the bands are greatly influenced by the neighboring bands in the spectrum when the perturbation is small, and can be approximately treated to be decoupled with the rest of the system [30]. Then we can rewrite Eq. (6) for a two-band system, especially with doubly degenerate states,

$$\begin{bmatrix}\omega_1 & 0\\ 0 & \omega_2\end{bmatrix}\boldsymbol{\alpha} - (\mathbf{k}-\mathbf{k}_0)\cdot\begin{bmatrix}0 & \boldsymbol{\kappa}_{12}\\ \boldsymbol{\kappa}^*_{12} & 0\end{bmatrix}\boldsymbol{\alpha} = \omega\begin{bmatrix}q_{11}+1 & q_{12}\\ -q^*_{12} & q_{22}+1\end{bmatrix}\boldsymbol{\alpha}, \tag{10}$$

where $\mathbf{k} = (k_x, k_y)$, $\boldsymbol{\kappa}_{mn} = (\kappa_{mn,x}, \kappa_{mn,y})$. Keep in mind that the second term of the left-hand side before $\boldsymbol{\alpha}$ is a dot product operation between $(\mathbf{k}-\mathbf{k}_0)$ and each element of matrix $\boldsymbol{\kappa}$. Given $\mathbf{k} = \mathbf{k}_0$, Eq. (10) of the non-Hermitian PCs is an alternative formulation of the Maxwell equations (1) and (2). Definitely, we can easily extend the two-component equation to three or more concerning the realistic concern, which we will discuss in detail in the following.

III. EXISTENCE OF A FLAT BAND AND ITS INTERACTION WITH $\mathcal{PT}$-SYMMETRIC POTENTIALS

Firstly, we focus on the presence of a flat band in a simple two-dimensional PC consisting of a square lattice. Obviously, at the center of the BZ there exist two degenerate states, i.e., two dipolar modes protected by the symmetry of the unit cell, as shown in Fig. 1(a). Referring to Eq. (10), the coupling constants $\boldsymbol{\kappa}_{12}$ between these two modes are absent; therefore, another adjacent state, a monopole mode, must be involved to investigate the evolution of these bands. Further expanding Eq. (10) to include three bands, the corresponding coupled

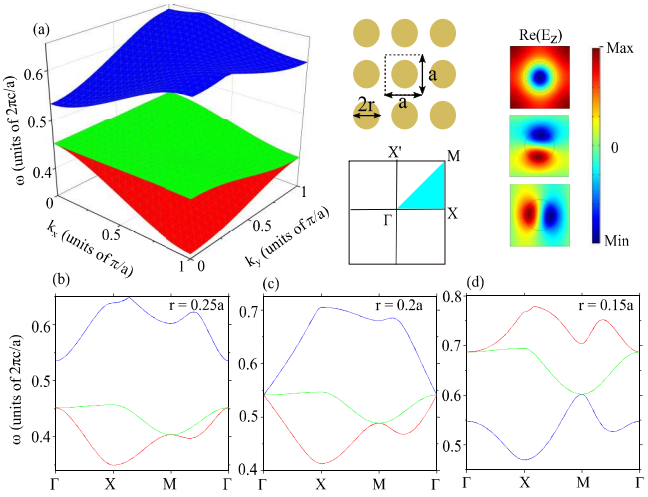

FIG. 1. (a) The "TM" band structure for Hermitian PCs formed of dielectric rods with $r = 0.25a$. The square array of the unit cell, the schematic plot of the BZ, and the field distribution for these three bands at the Γ point are shown in the right panel of (a). (b)–(d) are the dispersion for $r = 0.25a$, $0.2a$, and $0.15a$, respectively. The corresponding parameters are lattice constant a, relative permittivity of rods $\varepsilon_r = 12.5$, and relative permeability $\mu = 1$. All the results are obtained by the finite element method (FEM). The red, green, and blue lines correspond to the x-oriented and y-oriented dipolar states, and the monopole state, respectively.

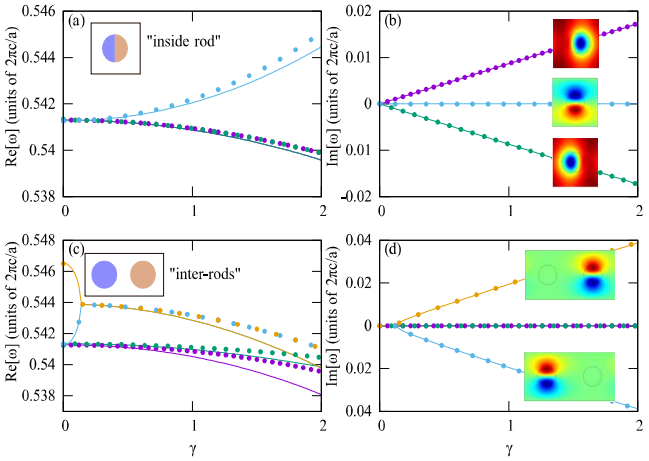

FIG. 2. (a), (c) Real and (b), (d) imaginary parts of the eigenfrequencies for the states near $f = 0.541(c/a)$ at the Γ point for cases where gain and loss are distributed in the unit cell as the inset of (a), (c), respectively. The solid lines are obtained by FEM, and the dots are obtained by the Hamiltonian equation (6). Different colors correspond to different bands.

mode equation reads

$$\begin{bmatrix} \omega_1 & 0 & 0 \\ 0 & \omega_2 & 0 \\ 0 & 0 & \omega_3 \end{bmatrix} \boldsymbol{\alpha} - \mathbf{k} \cdot \begin{bmatrix} 0 & 0 & \boldsymbol{\kappa}_{13} \\ 0 & 0 & \boldsymbol{\kappa}_{23} \\ \boldsymbol{\kappa}_{13}^* & \boldsymbol{\kappa}_{23}^* & 0 \end{bmatrix} \boldsymbol{\alpha} = \omega \boldsymbol{\alpha}, \quad (11)$$

where $\omega_1 = \omega_2 = \omega_0$. Only considering the Γ-X direction, i.e., $\mathbf{k} \to k_x$, $\boldsymbol{\kappa}_{13} \to \kappa_{13x}$, and $\boldsymbol{\kappa}_{23} \to \kappa_{23x}$, we can obtain the eigenvalues of Eq. (11) as

$$\omega = \omega_0, \frac{\omega_0 + \omega_3 \pm \sqrt{(\omega_0 - \omega_3)^2 + 4k_x^2(|\kappa_{13x}|^2 + |\kappa_{23x}|^2)}}{2}. \quad (12)$$

Apparently, there exists a flat band along the Γ-X direction belonging to the y-oriented dipolar mode, labeled as green curves in Figs. 1(b)–1(d). Similarly, the dispersion is also flat along the Γ-X' direction. Through Figs. 1(b)–1(d), we can conclude that this flat band exists for a wide range of the radius of the rods, indicating the robustness of this flat band. In particular, a triply degenerate point occurs at $r = 0.2a$ as shown in Fig. 1(c), which has been widely explored for the zero-index medium [31]. At present, the considered triply degenerate states have been constructed, and this degeneracy is obtained by fine-tuned parameters that give rise to an accidental degeneracy. Then we mainly focus on this example to illustrate the effects of a flat band in the context of $\mathcal{PT}$ symmetry. The non-Hermitian elements act on the considered triply degenerate states, which can be well understood by the aforementioned Eq. (6) in the following.

Focusing on the triple degeneracy at the Γ point, we first introduce the gain and loss in a cylinder of a primitive cell with the configuration of $\varepsilon(\mathbf{r}) = \varepsilon^*(-\mathbf{r})$, i.e., $\varepsilon_i(x, y) = -\varepsilon_i(-x, -y) = \gamma$, as sketched in the inset (labeled "inside rod") in Fig. 2(a), where $x = 0$ represents the center of the cylinder. Figures 2(a) and 2(b) show the real and imaginary parts of the eigenfrequencies of the involved states as a function of the gain-loss strength γ, respectively. It is seen that $\mathcal{PT}$-symmetric transitions show up for two of these states once the gain and loss is present ($\gamma > 0$), i.e., a thresholdless $\mathcal{PT}$ transition. We also note that the imaginary parts of the eigenfrequencies of these two $\mathcal{PT}$-symmetric states are approximately in linear dependence on γ as shown in Fig. 2(b). To understand these intriguing $\mathcal{PT}$-symmetric features, we inspect the following eigenfunction from Eq. (6) for $\mathbf{k} = \mathbf{k}_0$ at the Γ point:

$$\omega\boldsymbol{\alpha} = \begin{bmatrix} q_{11} + 1 & q_{12} & q_{13} \\ -q_{12}^* & q_{22} + 1 & q_{23} \\ -q_{13}^* & -q_{23}^* & q_{33} + 1 \end{bmatrix}^{-1} \begin{bmatrix} \omega_1 & 0 & 0 \\ 0 & \omega_2 & 0 \\ 0 & 0 & \omega_3 \end{bmatrix} \boldsymbol{\alpha}. \quad (13)$$

Providing $q_{mn} = 0$ if $m = n$ due to the symmetry, $q_{12} = 0$ for two dipolar modes, and $\omega_1 = \omega_2 = \omega_3 = \omega_0$ for triple degeneracy, then the eigenvalues of Eq. (13) can be obtained as

$$\omega = \omega_0, \frac{\omega_0 \pm j\sqrt{\omega_0^2(|q_{13}|^2 + |q_{23}|^2)}}{(1 + |q_{13}|^2 + |q_{23}|^2)}. \quad (14)$$

It is clear that there exists a constant frequency ω_0 in Eq. (14), which belongs to the y-oriented dipolar state. This state is preserved to be constant, not affected by the involvement of the gain-loss distribution. Therefore, it is robust against the non-Hermitian element if the gain-loss profile is with opposite parity with respect to the field distribution.

In conjugation with Eq. (7), q_{mn} is directly proportional to the degree of non-Hermiticity γ. Referring to Eq. (14), we can conclude that the imaginary parts of the eigenfrequencies of the involved modes are linear with the function of γ, which can be clearly observed in Fig. 2(b). The formation of this thresholdless $\mathcal{PT}$-symmetric transition between these two modes is responsible for the accidental degeneracy and the nonzero of q_{13}, q_{23}. Note that the thresholdless $\mathcal{PT}$-breaking transition is subject to the symmetric profile of the gain-loss potential [28]. Here, the inversion symmetry and mirror symmetry are identical to determine the coupling elements. However, we stress that as the gain and loss increase, Eq. (13) is not accurate since the coupling effect with more bands needs to be taken into account. As a result, we have selected the lowest ten bands to implement Eq. (6) to investigate the evolution of the complex band structure, as shown in Fig. 2. The small mismatch of the real parts between the results of the finite element method (FEM, implemented by COMSOL Multiphysics) and Eq. (6) originates from the absence of the lowest band at the Γ point with nearly zero frequency in Eq. (6). However, the imaginary parts [see Figs. 2(b) and 2(d)] are in excellent agreement, which implies the validity of the selected finite bands to describe the evolution of the complex band structure.

For a different gain-loss distribution in the rods obeying $\varepsilon(\mathbf{r}) = \varepsilon^*(-\mathbf{r})$, i.e., $\varepsilon_i(x, y) = -\varepsilon_i(x + a, y) = \gamma$ as sketched in the inset labeled "inter-rods" in Fig. 2(c), the unit cell needs be considered including two primitive cells in terms of band structure calculation. The states belonging to the triple degeneracy are not coupled together anymore, as their corresponding coupling strength q_{mn} vanishes. Alternatively, two superstates originating from the folding of this flat band tend to be coupled, which can be described by Eq. (10) with $\mathbf{k} = \mathbf{k}_0$. Due to $\omega_1 \neq \omega_2$, the corresponding band structure experiences a general $\mathcal{PT}$ transition from the $\mathcal{PT}$-symmetric phase to the broken phase, as shown in Figs. 2(c) and 2(d). Furthermore, the small gap between ω_1 and ω_2 results in the absence of the EP with a quite small value of γ. At the EP, the Hamiltonian cannot be diagonalizable and becomes defective [26].

In Fig. 2 we have basically demonstrated the profound role of the gain and loss in the mode evolutions at the original degenerate point. To study the effects of gain and loss on the full momentum space and the transmission properties, we then fix $\gamma = 1$ to calculate the complex band structure. Figures 3(a) and 3(b) show the complex band structure for inside-rod gain-loss distribution. It is evident that the whole k space considered in this study is divided into two regions: (I) in the vicinity of the Γ point where the original triply degenerate states exist, real parts of eigenfrequencies are degenerate, while imaginary parts are complex conjugate; (II) away from the central region, all the states are in $\mathcal{PT}$-symmetric phase with purely real eigenfrequencies. This is actually a ring of EPs, similar to the previously observed spawning rings of EPs by radiation loss [24].

Figures 3(c) and 3(d) show the complex band structure for inter-rod gain-loss distribution. The corresponding Hermitian band structure of the supercell (periodicity doubled from the primitive rod cell) can be regarded as the folding band of the original unit cell [25,32]. Note that along the y direction in k space ($X \rightarrow M$), all the states are naturally doubly degenerate

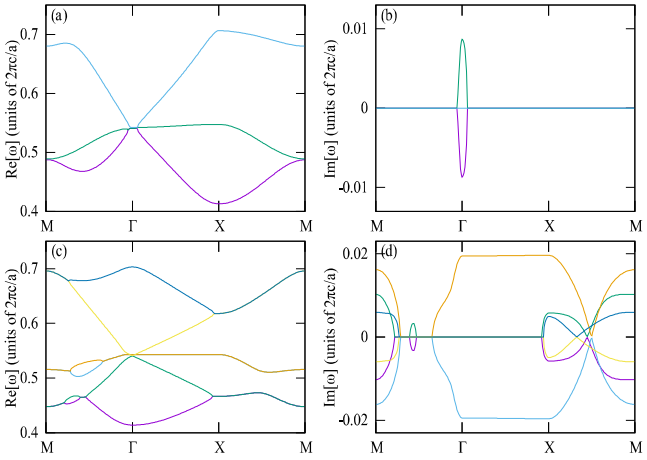

FIG. 3. Complex band structures for (a), (b) primitive cell and (c), (d) supercell near $f = 0.541(c/a)$. (a), (c) Left panels plot the real parts of the eigenfrequencies, and (b), (d) the right panels plot the imaginary parts. Different colors denote different band index.

because they locate on the band folding line $X \rightarrow M$ where $k_x = 0.5(\pi/a)$. If $\mathcal{PT}$-symmetric potentials are involved, exceptional contours are present starting from the boundaries of the BZ [25]. This explains why in the $X \rightarrow M$ direction, all states are in the $\mathcal{PT}$-broken phase [see Figs. 3(c) and 3(d)]. Notice that the original band for the y-oriented dipolar mode along $\Gamma \rightarrow X$ is approximately flat [see green lines in Figs. 1(b)–1(d)], resulting in it being almost overlapped after the band folding. Therefore a small non-Hermiticity potential γ would result in emergence of EPs. Apart from the flat band, the original linearly crossed bands forming the linear dispersion still hold in the vicinity of the Γ point because of their zero coupling strength q_{mn}, as shown in Fig. 3(c).

IV. TRANSMISSION PROPERTIES

Evidently, the band structure can be effectively modulated by the introduction of gain and loss, and thus determines the transmission of PCs. Subsequently, we proceed to examine the transmission properties of this PC slab with the properly engineered $\mathcal{PT}$ symmetry. Figure 4 shows the equifrequency contour which belongs to the flat band, and the analysis of transmission determined by group velocity $v_g = \nabla_k \omega(k)$ [23]. Together with the equifrequency contour of the Hermitian PCs [see Fig. 4(a)], when the incident plane wave with frequency $f = 0.541(c/a)$ is propagating with $\theta = 0°$, the PC slab exhibits the typical transmission property of zero-refractive material [31]. Obviously, it can also transport the incident waves for the other incident angle. The situation changes dramatically when we turn on the gain and loss. For the case of inside-rod gain-loss distribution whose band structure belonging to the green line of Fig. 3(a) is shown in Fig. 4(b), the $\mathcal{PT}$-broken region lies in the vicinity of the Γ point with frequency $f = 0.540\,89(c/a)$. Figure 4(b) shows that the corresponding equifrequency contour has a gap in the wave-vector space near $\theta = 81°$, which results in nearly zero transmission [cf. field distribution at $\theta = 81°$ in the inset of Fig. 4(d)]. On the contrary, the transmission is amplified

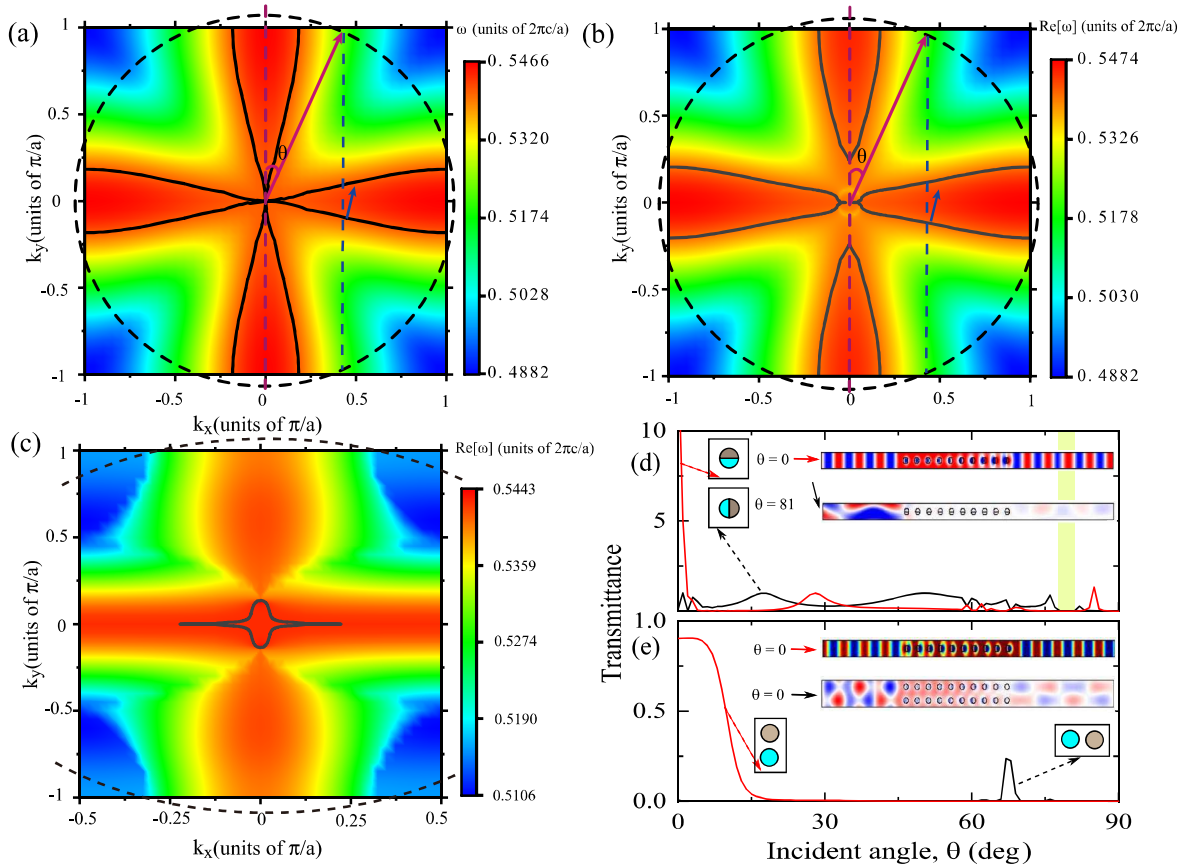

FIG. 4. The density plot of the real parts of the eigenfrequencies for the flat band: (a) Hermitian PCs, (b) non-Hermitian PCs with inside-rod gain-loss configuration, and (c) with inter-rod gain-loss configuration. The equifrequency contour (black solid lines) for a p-polarized plane wave source with $f = 0.541(c/a)$ (a), $f = 0.540\,89(c/a)$ (b), and $f = 0.542\,85(c/a)$ (c) incident upon a PC slab infinite in the x direction and with ten layers in the y direction. (d), (e) The transmittance for the corresponding lattice same as (b), (c), respectively, with different incident angle θ. The cell forming the PC slab is specified by the dashed arrows with their individual colors, and θ is the incident angle from the bottom port. The insets in (d), (e) are the field distribution E_z for characteristic angles. The black dashed curve and the black solid curve denote the equifrequency contours of air and PCs, respectively.

for the fundamental cell effectively rotated by 90° [see the red curves and the field distribution at $\theta = 0°$ in the inset of Fig. 4(d)]. In this case, a gain state locates in the $\mathcal{PT}$-broken region, which results in the enhancement of the field amplitude both for transmitted and reflected waves.

Significantly, for the case of inter-rod gain-loss distribution as shown in Fig. 3(c), the phenomena are quite different. From the density plot of the eigenfrequency belonging to the orange line of Fig. 3(c), Fig. 4(c) shows that the equifrequency contour for $f = 0.542\,85(c/a)$ is a closed contour around the BZ center. Simultaneously, it belongs to a flat band where $v_g \to 0$. The transmission for $f = 0.542\,85(c/a)$ should be forbidden. However, another equifrequency contour originating from another band with this specific frequency [cf. the yellow line in Fig. 3(c)] lies in the center of the Γ point, which is not shown in Fig. 4(c). In this case, the transmission for the x or y direction incidence recovers, as revealed by the transmission and the field distribution in the inset of Fig. 4(e). Simultaneously, all the contours for frequency $f = 0.542\,85(c/a)$ are located in the central BZ with a small span, which results in nearly zero transmission with a small incident angle.

V. CONCLUSIONS

In conclusion, we have theoretically and numerically investigated the existence of the Hermitian flat band and the associated mode coupling behaviors mediated by $\mathcal{PT}$ symmetry. In conjugation with the diverse gain-loss configurations, the degeneracy including the flat band has great effects on the behaviors of the general $\mathcal{PT}$-symmetric transition and thresholdless $\mathcal{PT}$ transition. All of these can be predicted and verified by a general coupled mode equation. Besides, different types of $\mathcal{PT}$-symmetric patterns, including the inside-rod and the inter-rod gain-loss symmetric distributions, yield effective control over the band structure, as well as intriguing angle-dependent transmission modulation such as zero-refractive and unidirectional amplification. Then it can be utilized in all-angle supercollimation and unidirectional behavior.

ACKNOWLEDGMENT

This work was supported by Shenzhen Municipal Science and Technology Plan (Grant No. JCYJ20170811154119292) and NSF of Guangdong Province (Grant No. 2015A030313748).

[1] H. S. Nguyen, F. Dubois, T. Deschamps, S. Cueff, A. Pardon, J.-L. Leclercq, C. Seassal, X. Letartre, and P. Viktorovitch, Phys. Rev. Lett. **120**, 066102 (2018).

[2] L. Morales-Inostroza and R. A. Vicencio, Phys. Rev. A **94**, 043831 (2016).

[3] B. Yang, T. Wu, and X. Zhang, J. Opt. Soc. Am. B **34**, 831 (2017).

[4] S. Mukherjee, A. Spracklen, D. Choudhury, N. Goldman, P. Öhberg, E. Andersson, and R. R. Thomson, Phys. Rev. Lett. **114**, 245504 (2015).

[5] X.-Y. Zhu, S. K. Gupta, X.-C. Sun, C. He, G.-X. Li, J.-H. Jiang, X.-P. Liu, M.-H. Lu, and Y.-F. Chen, Opt. Express **26**, 24307 (2018).

[6] L. Ge, Photonics Res. **6**, A10 (2018).

[7] B. Qi, L. Zhang, and L. Ge, Phys. Rev. Lett. **120**, 093901 (2018).

[8] D. Leykam, S. Flach, and Y. D. Chong, Phys. Rev. B **96**, 064305 (2017).

[9] C. M. Bender, Rep. Prog. Phys. **70**, 947 (2007).

[10] C. M. Bender and S. Boettcher, Phys. Rev. Lett. **80**, 5243 (1998).

[11] R. El-Ganainy, K. G. Makris, M. Khajavikhan, Z. H. Musslimani, S. Rotter, and D. N. Christodoulides, Nat. Phys. **14**, 11 (2018).

[12] L. Feng, R. El-Ganainy, and L. Ge, Nat. Photonics **11**, 752 (2017).

[13] N. Moiseyev, *Non-Hermitian Quantum Mechanics* (Cambridge University Press, Cambridge, 2011).

[14] W. D. Heiss, J. Phys. A: Math. Gen. **37**, 2455 (2004).

[15] Z. Liu, Q. Zhang, X. Liu, Y. Yao, and J.-J. Xiao, Sci. Rep. **6**, 22711 (2016).

[16] I. Rotter, J. Phys. A: Math. Theor. **42**, 153001 (2009).

[17] L. Feng, Z. J. Wong, R.-M. Ma, Y. Wang, and X. Zhang, Science **346**, 972 (2014).

[18] H. Hodaei, M.-A. Miri, M. Heinrich, D. N. Christodoulides, and M. Khajavikhan, Science **346**, 975 (2014).

[19] Z. Lin, H. Ramezani, T. Eichelkraut, T. Kottos, H. Cao, and D. N. Christodoulides, Phys. Rev. Lett. **106**, 213901 (2011).

[20] B. Peng, Ş. K. Özdemir, F. Lei, F. Monifi, M. Gianfreda, G. L. Long, S. Fan, F. Nori, C. M. Bender, and L. Yang, Nat. Phys. **10**, 394 (2014).

[21] W. Chen, Ş. Kaya Özdemir, G. Zhao, J. Wiersig, and L. Yang, Nature **548**, 192 (2017).

[22] H. Hodaei, A. U. Hassan, S. Wittek, H. Garcia-Gracia, R. El-Ganainy, D. N. Christodoulides, and M. Khajavikhan, Nature **548**, 187 (2017).

[23] J. D. Joannopoulos, S. G. Johnson, J. N. Winn, and R. D. Meade, *Photonic Crystals: Molding the Flow of Light*, 2nd ed. (Princeton University Press, Princeton, NJ, 2011).

[24] B. Zhen, C. W. Hsu, Y. Igarashi, L. Lu, I. Kaminer, A. Pick, S.-L. Chua, J. D. Joannopoulos, and M. Soljačić, Nature **525**, 354 (2015).

[25] A. Cerjan, A. Raman, and S. Fan, Phys. Rev. Lett. **116**, 203902 (2016).

[26] K. Ding, Z. Q. Zhang, and C. T. Chan, Phys. Rev. B **92**, 235310 (2015).

[27] J. Xu and Y. Chen, Opt. Express **23**, 22619 (2015).

[28] L. Ge and A. D. Stone, Phys. Rev. X **4**, 031011 (2014).

[29] K. Sakoda, *Optical Properties of Photonic Crystals*, 2nd ed. (Springer, Berlin, New York, 2005).

[30] S. Wu and J. Mei, AIP Adv. **6**, 015204 (2016).

[31] X. Huang, Y. Lai, Z. H. Hang, H. Zheng, and C. T. Chan, Nat. Mater. **10**, 582 (2011).

[32] Z. Z. Liu, F. Qin, Q. Zhang, and J. J. Xiao, Opt. Express **25**, 26689 (2017).